

## RECONSTRUCTION ALGORITHM FOR OBTAINING THE BENDING DEFORMATION OF THE BASE OF HEAVY-DUTY MACHINE TOOL USING INVERSE FINITE ELEMENT METHOD

Mingyao Liu<sup>1,2)</sup>, Xiong Zhang<sup>1,2)</sup>, Han Song<sup>1,2)</sup>, Jingliang Wang<sup>1,2)</sup>, Shiguang Zhou<sup>1,2)</sup>

1) Wuhan University of Technology, School of Mechanical and Electrical Engineering, Wuhan 430070, Hubei, China  
(lmylyf@126.com, ✉ 213821@whut.edu.cn, +86 136 6720 3163, 644099615@qq.com, 403239612@qq.com, 274760169@qq.com)

2) Hubei Digital Manufacturing Key Laboratory, Wuhan 430070, Hubei, China

### Abstract

The field of mechanical manufacturing is becoming more and more demanding on machining accuracy. It is essential to monitor and compensate the deformation of structural parts of a heavy-duty machine tool. The deformation of the base of a heavy-duty machine tool is an important factor that affects machining accuracy. The base is statically indeterminate and complex in load. It is difficult to reconstruct deformation by traditional methods. A reconstruction algorithm for determining bending deformation of the base of a heavy-duty machine tool using inverse Finite Element Method (iFEM) is presented. The base is equivalent to a multi-span beam which is divided into beam elements with support points as nodes. The deflection polynomial order of each element is analysed. According to the boundary conditions, the deformation compatibility conditions and the strain data measured by Fiber Bragg Grating (FBG), the deflection polynomial coefficients of a beam element are determined. Using the coordinate transformation, the deflection equation of the base is obtained. Both numerical verification and experiment were carried out. The deflection obtained by the reconstruction algorithm using iFEM and the actual deflection measured by laser displacement sensors were compared. The accuracy of the reconstruction algorithm is verified.

Keywords: inverse Finite Element Method, bending deformation, heavy-duty machine tool, reconstruction algorithm, statically indeterminate structure.

© 2018 Polish Academy of Sciences. All rights reserved

## 1. Introduction

A heavy-duty machine tool, a kind of high-precision general manufacturing equipment, is a key equipment which determines the strength of national aerospace, precision manufacturing and overall processing of large parts. It is of great significance to improve the machining precision of a heavy-duty machine tool. The mechanical and thermal deformation of the large structural parts of heavy-duty machine tool are the main factors that affect the machining precision, so real-time monitoring and compensation of the mechanical and thermal deformation of a heavy-duty machine tool are of great significance to improve the processing accuracy [1–4].

In the presented study, the methods for real-time monitoring and compensation of the deformation of large structural elements of a heavy-duty machine tool are divided into two parts, one

of which is the calculation of deformation, and the other is the measurement of deformation. The calculation of deformation is based on the *Finite Element Method* (FEM) which uses the force acting on the structure and the stiffness matrix to obtain the displacement field [5]. If the force acting on the structure and the stiffness matrix of the structure are given, the deformation of the structure can be obtained. The FEM has a simple algorithm, a fast dynamic response, accurate calculation and other merits. It is effective in dealing with the deformation of a simple structure under the action of a simple force. However, a heavy-duty machine tool is complex in load and shape, so it is difficult to obtain the force acting on it and the stiffness matrix calculated by the shape function. Due to the above shortcomings, the FEM has a limitation in reconstruction of the deformation of a heavy-duty machine tool.

In order to compensate for the shortcomings of FEM, the researchers put forward a proposal of measuring the deformation. It is also divided into two parts. One of them is the direct measurement, and the other is the indirect measurement. The direct measurement is performed mainly by the way of measuring the deformation field of a heavy-duty machine tool by laser displacement sensors, and its compensation [6]. Its advantages are easy operation, mature technologies and a simple principle. However, many of the aforementioned direct measurements of deformation have the following weaknesses: 1) the shape of heavy-duty machine tool structures is complex, so that it limits the distribution of laser displacement sensors; 2) since a large number of laser displacement sensors are placed over the structure surfaces to measure the deformation data of discrete points on the structures, the workload of data analysis and processing increases which makes the dynamic response of the system reduced. Because of the above shortcomings, the direct measurement of deformation fails to fulfil the requirements of real-time monitoring and compensation of a heavy-duty machine tool.

The indirect measurement of deformation uses resistance strain sensors or FBG to obtain strain data or temperature data and to transform them into a displacement field which is based on iFEM. The core of iFEM is to monitor, reconstruct and compensate the mechanical and thermal deformation of the structure by using the strain information from a set of FBG sensors mounted to the surface of structural parts [7–9]. Tessler A., *et al.* (2005) obtained a variational principle formulated for the inverse problem of full-field reconstruction of three-dimensional plate/shell deformations from experimentally measured surface strains. The formulation was based upon the minimization of a least-squares functional that used the complete set of strain measures consistent with the linear, first-order shear-deformation theory [10]. Marco Gherlone, *et al.* (2012) presented a computational method based on iFEM to reconstruct both static and time-varying displacement fields of truss, beam, and frame structures by using the measured surface-strain data [9]. Similarly, in 2014, Marco Gherlone *et al.* further demonstrated that iFEM applied to beam and frame structures is reliable when the experimentally measured strains are used as the input data [11]. Priscilla Cerracchio, *et al.* (2015) reconstructed the displacement of typical composite stiffened structures which were under the static, dynamic, and thermal loadings using iFEM [12]. Adnan Kefal, *et al.* (2016, 2018) successfully used iFEM based on a four-node inverse quadrilateral shell (iQS4) element to perform the displacement and stress monitoring of a typical chemical tanker mid-ship [13], a Panamax containership [14] and bulk carriers [15]. Moreover, the new four-node quadrilateral inverse-shell element, iQS4, which includes hierarchical drilling rotation *degrees-of-freedom* (DOF) was developed by Adnan Kefal, *et al.* (2016) and it can further extend the practical usefulness of iFEM [16]. Furthermore, Adnan Kefal, *et al.* (2017) presented an improved iFEM formulation which includes the kinematics of Refined Zigzag Theory (RZT) to monitor the displacement and stress field of laminated composite, sandwich plates, shells [17] and airplane-wing-shaped thick panels [18]. Marco Gherlone, *et al.* (2018) separately used iFEM, the Modal Method and Ko's Displacement Theory to reconstruct the displacement

of a cantilevered, wing-shaped aluminium plate. By comparing the three reconstruction results, iFEM is proved to be slightly more accurate and particularly attractive [19].

The real-time acquisition of the strain data is the key component of iFEM. An FBG sensor has a high sensitivity to the change of temperature and strain, so it is used to measure the strain data of a heavy-duty machine tool [20, 21]. In order to obtain the accurate deformation of a heavy-duty machine tool, reliability of FBG strain values at measured points and selection of temperature-sensitive measuring points are critical to the measurement results of strain and temperature field [22–26]. The traditional iFEM can obtain the deformation of a structural part without knowing the magnitude and form of the force acting on it by using a theoretical analysis, so it has a good application prospect in real-time monitoring and compensation of the mechanical and thermal deformation of a heavy-duty machine tool. However, it can only obtain the deformation of some simple structural parts [27–30]. In the actual situation, the base of a heavy-duty machine tool is a statically indeterminate structure, and using the traditional iFEM it is difficult to obtain the deformation.

The base of a heavy-duty machine tool is statically indeterminate and complex in load. Because the information on support forces and a force acting on the base is difficult to obtain, the above methods fail to fulfil the requirements. This paper presents a reconstruction algorithm for obtaining the bending deformation of the base of a heavy-duty machine tool using iFEM. The base is divided into beam elements with support points as nodes. The beam element deflection can be expressed by a polynomial, and the polynomial coefficients can be determined according to the boundary conditions, the deformation compatibility conditions and the strain data measured by FBG. Using the coordinate transformation, the deflection equation of the base is obtained. The reconstruction algorithm has the following advantages: 1) it can reconstruct the deflection of the base of a heavy-duty machine tool without considering the magnitude and form of the force acting on it; 2) it can reconstruct the deflection of the base which is statically indeterminate and complex in load. The reconstruction algorithm presents a new method for the real-time monitoring and compensation of deformation of structural parts of a heavy-duty machine tool, which is of great significance to improving the machining precision of a heavy-duty machine tool.

In the remainder of the paper, the kinematic assumptions for the element are discussed, followed by a description of the reconstruction algorithm of the base using iFEM (Section 2). The numerical verification is presented in Section 3. The method and experiment setup are then discussed (Section 4). Finally, to examine the predictive capability of the reconstruction algorithm using iFEM, an experiment was performed on a model of the base under the action of unknown forces. The deflection obtained by the reconstruction algorithm using iFEM and the actual deflection measured by laser displacement sensors were compared (Section 5). The conclusions of this research are presented in Section 6.

## 2. Principle of reconstruction algorithm

The key step in the reconstruction algorithm is to determine the order and evaluate the coefficients of the deflection polynomial. In this section, the deflection polynomial order of each beam element is analysed and the deflection polynomial coefficients are determined. The base of a heavy-duty machine tool is equivalent to a multi-span beam shown in Fig. 1. It is divided into beam elements,  $1_{st}, 2_{st}, \dots, m_{st}$ , with support points as nodes. In Fig. 1,  $F_1, F_2, \dots, F_m$  are forces acting on  $1_{st}, 2_{st}, \dots, m_{st}$  elements, respectively;  $(x_1, y_1), (x_2, y_2), \dots, (x_m, y_m)$  are local coordinate systems of beam elements;  $l_1^e, l_2^e, \dots, l_m^e$  are lengths of  $1_{st}, 2_{st}, \dots, m_{st}$  elements, respectively, and  $N_i$  ( $i = 1, 2, \dots, m+1$ ) are nodes.

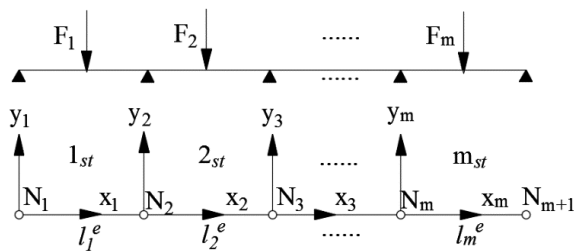


Fig. 1. The equivalent model and elements of the base.

### 2.1. Order of deflection polynomial

The  $j_{st}$  ( $j = 1, 2, \dots, m$ ) beam element of a multi-span beam is shown in Fig. 2. The three Cartesian components of the displacement vector are consistent with the kinematic assumptions that the section of the element is flat before deformation and remains flat after deformation, but rotates within an angle around the neutral axis and remains orthogonal to the axis of the element [9]. Based on the above assumptions, the displacement field of the element under the action of unknown force along Z axis can be expressed as follows:

$$u_x(x, y, z) = z \theta_y(x), \tag{1a}$$

$$u_y(x, y, z) = 0, \tag{1b}$$

$$u_z(x, y, z) = w(x), \tag{1c}$$

where  $u_x, u_y, u_z$  are displacements along  $x, y,$  and  $z$  axes, respectively, with  $w$  denoting a displacement at  $y = z = 0$ ;  $\theta_y$  is a rotation about  $Y$  axis; positive orientations for the displacements and rotations are depicted in Fig. 2.

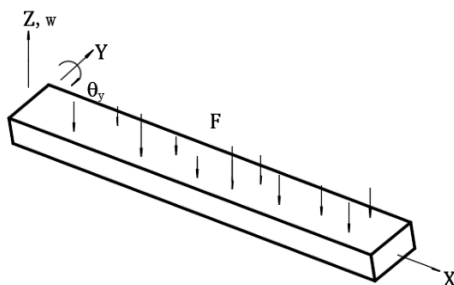


Fig. 2. The deformation component of the element.

Using the geometric equation, the strain field of the element can be expressed as follows:

$$\epsilon_x(x, y, z) = z \frac{dw^2(x)}{dx^2} = z \frac{d\theta_y(x)}{dx} = z \kappa_1(x), \tag{2a}$$

$$\gamma_{xz}(x, y) = \frac{dw(x)}{dx} + \theta_y(x) = \kappa_2(x), \tag{2b}$$

$$\gamma_{xy}(x, z) = 0, \tag{2c}$$

where  $\kappa_1(x)$  and  $\kappa_2(x)$  are section strains.

As shown in Fig. 3, according to the constructive equations, the section force  $Q_z$  and its moment  $M_y$  can be expressed as follows:

$$Q_z = G_z \kappa_2, \tag{3a}$$

$$M_y = D_y \kappa_1, \tag{3b}$$

where  $G_z$  is shear rigidity and  $D_y$  denotes bending rigidity.

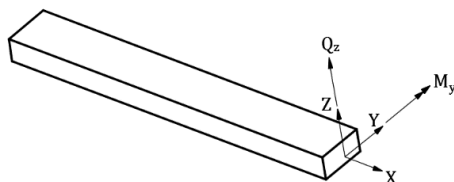


Fig. 3. The section force and moment of the element.

Using the equilibrium functions, the relations between the section force and its moment and the distributed load  $q_z$  along Z direction are:

$$\frac{dQ_z}{dx} + q_z = 0, \tag{4a}$$

$$\frac{dM_y}{dx} - Q_z = 0. \tag{4b}$$

Consider one of the beam elements loaded by a uniformly distributed transverse force  $q_z$ . For a loaded element, the distributed load is constant,  $q_z = const$ . Whereas the section force  $Q_z$  is linear, the section moment  $M_y$  is quadratic (refer to (4a), (4b)). (3a) indicates that the section strain  $\kappa_1$  is quadratic. From (2a), it is deduced that the deflection polynomial of a loaded element,  $w(x)$ , is quartic.

For an unloaded element, the distributed load is zero,  $q_z = 0$ . After substituting  $q_z$  into (4a), it is deduced that  $Q_z$  needs to be constant and  $M_y$  linear. The section strain  $\kappa_1$  remains linear. As in (2a), the deflection polynomial of a loaded element,  $w(x)$ , is cubic.

According to the aforementioned analysis, it is deduced that the deflection polynomial of a loaded element is quartic and of an unloaded element – cubic. This conclusion will be used in the following analysis (Subsection 2.2, (5) and (12)).

## 2.2. Inverse Finite Element Method for beam

According to Subsection 2.1, the deflection polynomial order of an element can be determined. In this section, using the boundary conditions, the deformation compatibility conditions and the relation between the strain data measured by FBG and the deflection of element, the deflection polynomial coefficients of element are obtained. By using the coordinate transformation, the deflection of the base can be determined.

In a local coordinate system  $(x_1, y_1)$  the deflection polynomial of  $1_{st}$  element can be expressed as follows:

$$w_1^{(e)}(x) = \sum_{i=0}^n a_i x^i = N * \mathbf{a}, \tag{5}$$

where:  $N = (1, x, \dots, x^i)$  is a shape function;  $\mathbf{a}$  is a coefficient matrix of  $w_1^{(e)}$ .  $a_i$  are coefficients of the deflection polynomial; if the element is loaded,  $n = 4$ ; if the element is unloaded,  $n = 3$  (refer to the conclusion formulated in Subsection 2.2).

The relation between the deflection and the analytical strain data can be described as follow:

$$\left. \frac{d^2 w_1^{(e)}(x)}{dx^2} \right|_{x=x_i} = -\frac{\epsilon_1(x_i)}{z}, \tag{6}$$

where  $\epsilon_1(x_i)$  is an analytical strain,  $z$  is a distance from the location of analytical strain to the neutral surface.

According to (6), the relation between  $\mathbf{a}$  and the analytical strain data can be described as follows:

$$\epsilon_1(x_i) = -z * \frac{\partial^2 N}{\partial x^2} * \mathbf{a} = \mathbf{B}(x_i) * \mathbf{a}, \tag{7}$$

where  $\mathbf{B}(x_i)$  is a strain matrix which contains derivatives of the shape function.

A least square function  $\Phi$  containing the strain data  $\epsilon_1(x_i)^*$  acquired by FBG, and the analytical strain data  $\epsilon_1(x_i)$  are presented. The function can be written as:

$$\Phi = \|\epsilon_1(x_i) - \epsilon_1(x_i)^*\|^2. \tag{8}$$

The squared form of the above equation is following:

$$\Phi = \frac{L}{n} \sum_{i=1}^n [\epsilon_1(x_i) - \epsilon_1(x_i)^*]^2 = \frac{L}{n} \sum_{i=1}^n [\mathbf{B}(x_i) * \mathbf{a} - \epsilon_1(x_i)^*]^2, \tag{9}$$

where  $L$  is a length of the element,  $n$  is a number of the element.

In order to solve  $\mathbf{a}$ , (9) can be minimized with reference to  $\mathbf{a}$ , giving rise to:

$$\frac{\partial \Phi}{\partial \mathbf{a}} = \mathbf{k} \mathbf{a} - \mathbf{f} = 0, \tag{10}$$

where:  $\mathbf{k} = \frac{L}{n} \sum_{i=1}^n \mathbf{B}(x_i)^T \mathbf{B}(x_i)$ ,  $\mathbf{f} = \frac{L}{n} \sum_{i=1}^n \mathbf{B}(x_i)^T \epsilon_1(x_i)^*$ .

Because the nodes of element are support points of the base, according to the boundary conditions,  $w_1^{(e)}(0) = w_1^{(e)}(l_1^e) = 0$ , using (10), the deflection polynomial coefficients  $a_i$  can be obtained as follows:

$$\mathbf{a} = \mathbf{k}^{-1} \mathbf{f}. \tag{11}$$

In a local coordinate system  $(x_j, y_j)$  ( $j \geq 2$ ), the deflection polynomial of  $j_{st}$  element can be given by:

$$w_j^{(e)}(x) = \sum_{i=0}^n b_i x^i, \tag{12}$$

where  $n = 4$  if the element is loaded, and  $n = 3$  if the element is unloaded (refer to the conclusion drawn in Subsection 2.1).

The boundary conditions which are the same as those of  $1_{st}$  element are given by:

$$w_j^{(e)}(0) = w_j^{(e)}(l_j^e) = 0. \tag{13}$$

According to the deformation compatibility conditions, the rotations of  $(j-1)_{st}$  and  $j_{st}$  element,  $\theta_y$ , at node  $N_j$  are equal. It can be expressed as follows:

$$\frac{dw_{j-1}^{(e)}(x)}{dx} \Big|_{x=l_{j-1}^e} = \frac{dw_j^{(e)}(x)}{dx} \Big|_{x=0} \quad (14)$$

According to (13), (14), using iFEM described by (7)–(11), the deflection polynomial coefficients of  $j_{st}$  element,  $b_i$ , are deduced.

Transforming the local coordinate system  $(x_j, y_j)$  into  $(x_1, y_1)$ , the deflection of the base can be expressed as follows:

$$w(x) = \begin{cases} w_1^{(e)}(x) & (0 \leq x \leq l_1^e) \\ w_j^{(e)}\left(x - \sum_1^{j-1} l_k^e\right) & \left(\sum_1^{j-1} l_k^e \leq x \leq l_j^e + \sum_1^{j-1} l_k^e\right) \end{cases} \quad (15)$$

Because the base of a heavy-duty machine tool is statically indeterminate, the reaction forces are difficult to obtain, especially for a high-order statically indeterminate structure. The reconstruction algorithm using iFEM can reconstruct any high-order statically indeterminate structure. Many structural parts on the base of a heavy-duty machine tool make it complex in load, but the reconstruction algorithm can reconstruct the base under any loading without the information on the load.

In this paper, the accuracy of deflection which is obtained by the reconstruction algorithm is discussed when an unknown force is acting on the base. The numerical and experimental verifications are presented in Sections 3, 4 and 5.

### 3. Numerical verification

In this section, the strain data obtained from FEM analysis are used as the experimental strain data in iFEM analysis. iFEM and FEM displacements are compared to verify the accuracy of iFEM.

The numerical verification for three cases: a clamped edge beam and clamped-clamped beams with the measured points located at  $x = L/4$  and  $x = 3L/4$ , all subjected to a transverse pressure applied to the top surface, is presented. The beam was made of steel having Young’s modulus of 210 GPa and Poisson’s ratio of 0.3. The length of beam was 1250 mm, its width –40 mm and its height –15 mm. To model the beam, Hex dominant elements were employed. The information on elements and nodes of ANSYS simulation is shown in Table 1. Fig. 4 shows the result of mesh division.

Table 1. The information on elements and nodes in ANSYS simulation.

Element type	No. of elements along the beam section	No. of elements along the beam length	Total No. of elements	No. of nodes
Hex dominant	24	250	6000	32845

A pressure of 0.0001 MPa was applied to the top surface of the beam in the three numerical cases. In the first case, one end of the beam was clamped and the other was free. In the second case, the ends of the beam were all clamped with the measured point located at  $x = L/4$ .

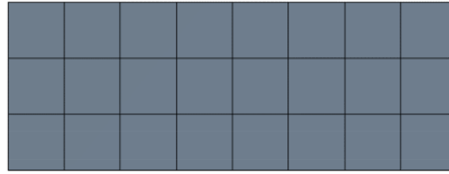


Fig. 4. The mesh division result of beam.

In the third case, the ends of the beam were all clamped with the measured point located at  $x = 3L/4$ . The constraint form and strain measurement distributions of the three cases are shown in Figs. 5a–5c, respectively. Using the strain data obtained by ANSYS simulation as input, the displacement of beam can be reconstructed by iFEM mentioned in Section 2 and are compared with the displacement obtained by ANSYS (direct FEM). Figs. 6a–6c show the comparison results between direct FEM and iFEM of the three numerical cases.

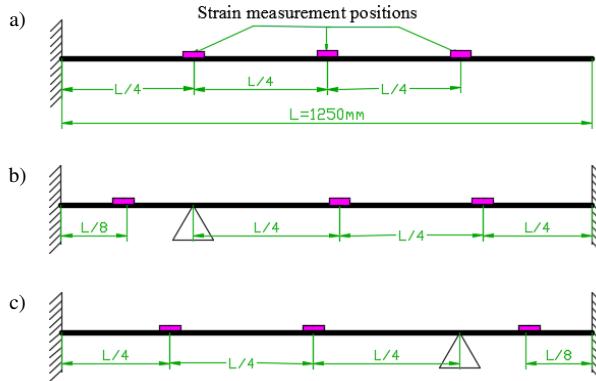


Fig. 5. a) The constraint form and strain measurement distributions of the beam in the first case; b) the constraint form and strain measurement distributions of the beam in the second case; c) the constraint form and strain measurement distributions of the beam in the third case.

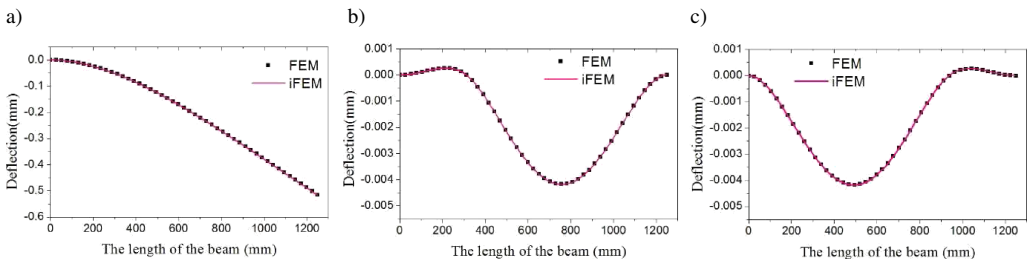


Fig. 6. a) The comparison results of direct FEM and iFEM in the first case; b) the comparison results of direct FEM and iFEM in the second case; c) the comparison results of direct FEM and iFEM in the third case.

According to the results found in the three numerical cases, the deflection obtained by ANSYS (direct FEM) is in good agreement with that reconstructed by iFEM.

## 4. Method and experiment setup

In this section, the operating principle of FBG and the method of experiment which was carried out to evaluate the applicability of the reconstruction algorithm are discussed.

### 4.1. Operating principle of FBG

FBG is a periodically distributed structure with a refractive index formed in fibre by exposure to UV, as shown in Fig. 7. When a beam of light is applied to the fibre grating, the periodicity of the refractive index allows only a specific wavelength of light to be reflected. The reflection wave length satisfies the Bragg scattering condition which can be expressed as follows:

$$\lambda_B = 2n\Lambda, \quad (16)$$

where  $n$  and  $\Lambda$  are an effective refractive index of grating and a grid period.

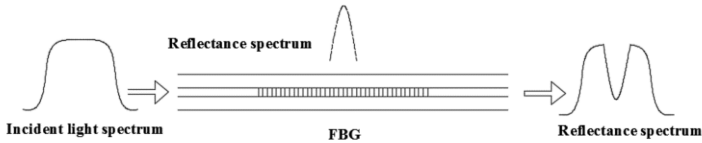


Fig. 7. The structure and reflection principle of FBG.

When a fibre grating is subjected to a pull force, the reflection wavelength of the fibre grating is influenced by the deformation caused by the pull force and the change of refractive index of optical fibre caused by the photo-elastic effect. The relation between the wavelength change of fibre grating and the strain is:

$$\frac{\Delta\lambda_B}{\lambda_B} = (1 - P_e) \cdot \varepsilon, \quad (17)$$

where  $P_e$  is an effective photo-elastic coefficient and the effective photo-elastic coefficient of an ordinary optical fibre is 0.22.

### 4.2. Method of experiment

As shown in Fig. 8, the base of a heavy-duty machine tool is equivalent to a two-span beam and the material parameters of it are shown in Table 2. The neutral axis of the base was used as

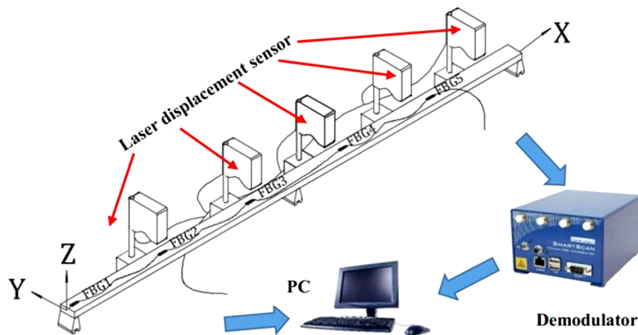


Fig. 8. A model of the experiment setup.

x-axis, and the coordinate system was established at the left end of the base. Five FBGs were mounted on the top surface of the base to measure the strain data. Three FBGs were mounted on  $1_{st}$  element and two FBGs were mounted on  $2_{st}$  element. When unknown forces were applied to the beam, the centres of wavelengths of FBGs were changed. The changes were measured and stored into PC by a demodulator. At the same time, laser displacement sensors were used to measure the actual deflection of given points on the base and to transmit them to PC. Then, the deflection polynomial of the base which was obtained by the reconstruction algorithm mentioned in Section 2 was compared with the actual deflection measured by the laser displacement sensors. By comparison, the accuracy of reconstruction algorithm for obtaining the bending deformation of the base of a heavy-duty machine tool using iFEM was examined. The centres of wavelengths and distributions of FBGs are shown in Table 3 and the distributions of points measured by the laser displacement sensors are shown in Table 4.

Table 2. The material parameters of the beam.

$l_i^{(e)}$ ( $i = 1, 2$ ) [mm]	Width [mm]	Height [mm]	Young's modulus [Pa]
625	40	15	$2.1 \times 10^{11}$

Table 3. The centres of wavelengths and distributions of FBGs.

FBG notation	Orientation of FBG	Wavelength centre [nm]	FBG notation	Orientation of FBG	Wavelength centre [nm]
1	(65, 0, 7.5)	1547	4	(815, 0, 7.5)	1553
2	(315, 0, 7.5)	1549	5	(1065, 0, 7.5)	1555
3	(565, 0, 7.5)	1551			

Table 4. The distributions of points measured by the laser displacement sensors.

Notation	Orientation of measured points	Notation	Orientation of measured points
1	(65, 0, 7.5)	5	(715, 0, 7.5)
2	(233, 0, 7.5)	6	(883, 0, 7.5)
3	(355, 0, 7.5)	7	(1005, 0, 7.5)
4	(507, 0, 7.5)	8	(1157, 0, 7.5)

## 5. Verification test

Figure 9 shows a photo of the experiment setup. The laser displacement sensor was used to measure the bending deformation of the base directly. The loaded weights were put on the loading station. The demodulator was used to measure the change of FBG wavelength centre and the PC was used to receive the data from the laser displacement sensor and the demodulator.

In order to examine the robustness and repeatability of the reconstruction algorithm, complex stress conditions of the base whose two elements were both loaded are presented (Fig. 10a). When the weights were put on the loading station, the strain data were obtained by FBG and the bending deformation of the base could be calculated using the reconstruction algorithm. At the same time, the bending deformation of the base also could be measured directly by the laser

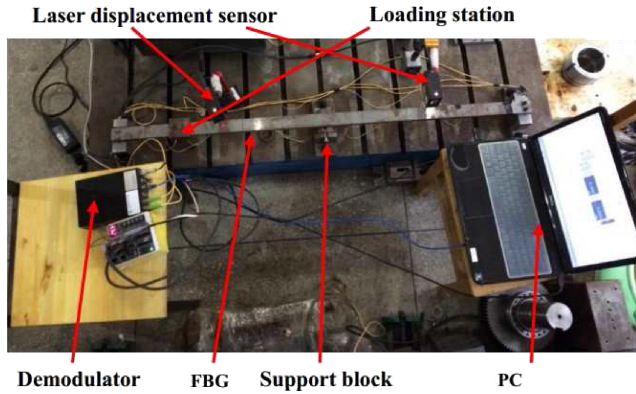


Fig. 9. The experiment setup.

displacement sensors. According to the reconstruction algorithm using iFEM mentioned in Section 2, the comparison of the deflection polynomial obtained by the reconstruction algorithm and the deflection of given points measured by the laser displacement sensors is shown in Fig. 10b.

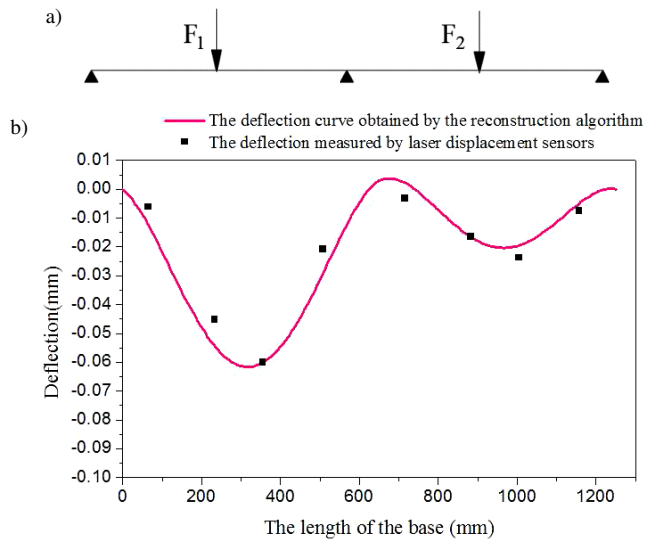


Fig. 10. a) The stress conditions of the base; b) a comparison of the deflection reconstructed by iFEM and that measured by the laser displacement sensors.

Figure 10b displays the reconstruction result when two elements were loaded. It shows that the deflection polynomial of the base obtained by the reconstruction algorithm well coincides with the actual deflection measured by the laser displacement sensors. Fig. 11 shows that the experimental discrete strain is in good agreement with the iFEM-based reconstructed continuous strain curve. The results prove that the reconstruction algorithm for obtaining the bending deformation of the base of a heavy-duty machine tool using iFEM is accurate. In the next step an error is analysed.

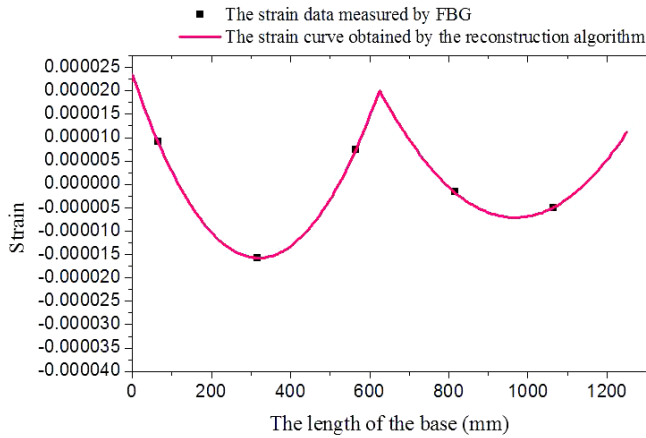


Fig. 11. A comparison of the strain data measured by FBG and reconstructed by iFEM.

As shown in Fig. 12, because it is difficult to ensure that FBG is clung to the top surface of the base when it was mounted, the strain data measured by FBG contain some errors when the base is deformed.

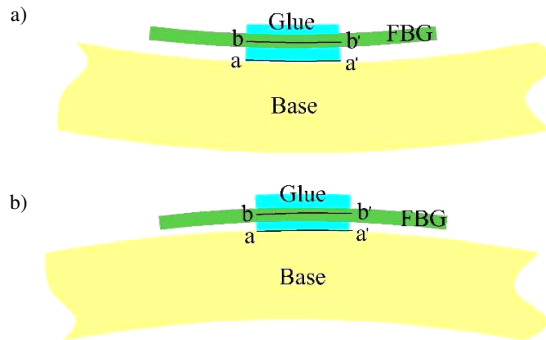


Fig. 12. a) The actual measuring position when FBG is pressed; b) the actual measuring position when FBG is pulled.

As shown in Fig. 12a, when FBG is pressed, the measuring position of FBG is represented by the  $b - b'$  cross-section, while the actual deformation position of the base is represented by the  $a - a'$  cross-section. The relation between the strain data for the two positions can be expressed as follows:

$$|\epsilon_{aa'}^-| < |\epsilon_{bb'}^-|, \quad (18)$$

where  $\epsilon_{aa'}^-$  is the actual strain of the base when it is pressed,  $\epsilon_{bb'}^-$  is the strain data measured by FBG.

As shown in Fig. 12b, when FBG is pulled, the relation between the strain data for the two positions is given by:

$$|\epsilon_{aa'}^+| < |\epsilon_{bb'}^+|, \quad (19)$$

where  $\epsilon_{aa'}^+$  is the actual strain of the base when it is pulled,  $\epsilon_{bb'}^+$  is the strain data measured by FBG.

For the above reasons, the reconstruction algorithm contains some errors when it uses the strain data measured by FBG. Of course, the laser displacement sensors also contain some measurement errors.

## 6. Conclusions

The deformation of the base of a heavy-duty machine tool is the main factor that affects the machining accuracy. Because the base is statically indeterminate and complex in load, it is difficult to obtain its deflection with the traditional methods. In search of a suitable method to use in real-time monitoring and compensation of deformation of the base of a heavy-duty machine tool, a reconstruction algorithm using iFEM is proposed. The base is divided into beam elements, and the deflection polynomial order of an element is determined by using the Timoshenko beam theory basic equations. The coefficients of deflection polynomial are obtained by using the boundary conditions, the deformation compatibility conditions and the relation between the strain data measured by FBG and the deflection of the element. The reconstruction algorithm can fulfil the requirements of real-time monitoring and compensation of deformation of the base of a heavy-duty machine tool.

In order to examine the accuracy of the reconstruction algorithm, a numerical verification and an experiment were carried out. The deflection polynomial obtained by the reconstruction algorithm was compared with the deflection of given points on the base measured by laser displacement sensors and the accuracy of the reconstruction algorithm was verified.

The reconstruction algorithm for obtaining the bending deformation of the base of a heavy-duty machine tool using iFEM can accurately reconstruct the deflection of the base under the action of unknown forces. It provides a theoretical basis for improving the machining precision of a heavy-duty machine tool.

## Acknowledgements

This experimental study was supported by the National Natural Science Fund of China (General Program, Grant #51375359), the International Cooperation Project of Hubei (Grant #2015DFA70340) and the Excellent Dissertation Cultivation Funds of Wuhan University of Technology (Grant #2016-YS-030). The authors would like to thank Hubei Digital Manufacturing Key Laboratory (Wuhan University of Technology) for providing the experiment equipment to accomplish the project. The authors also wish to gratefully acknowledge the assistance of Lan Feng, Dong Ai, Yuanming Fang, Wei Chen and Xuemin Zhang in the experiment.

## References

- [1] Xiong, Y., Wu, J., Deng, C. (2016). Machining process parameters optimization for heavy-duty CNC machine tools in sustainable manufacturing. *Int. J. Adv. Manuf. Technol.*, 87(5–8), 1237–1246.
- [2] Cui, G.W., Cheng, F.L., Gao, D. (2011). Real-Time Compensation of Ram Thermal Elongation Errors for Heavy-Duty Numerical Control Machine Tool. *Advanced Materials Research*, 317–319, 1964–1967.
- [3] Cheng, F.L., Jiang, B., Li, Y. (2012). The Analysis and Evaluation Method of Assembly Accuracy Reliability of Heavy Duty Machine Tool. *Advanced Materials Research*, 500, 608–613.

- [4] Jiang, B., Zhao, J.X., Sun, S.Z. (2014). Design Method of Assembly Accuracy Repeatability of Heavy Duty Machine Tool. *MATER SCI FORUM*, 800–801, 516–520.
- [5] Lu, Y., Cui, G.W., Gao, D. (2012). Thermal Deformation Finite Element Analysis for the Ram of Heavy-Duty CNC Machine Tools. *Advanced Materials Research*, 433–440, 7159–7164.
- [6] Liu, M., Wang, L., Kang, Y. (2016). Study on the deformation measurement and reconstruction of heavy-duty machine column based on FBG sensor. *IEEE International Conference on Mechatronics and Automation, IEEE*, 1221–1225.
- [7] Xu, Y., Chan, L.C., Tsien, Y.C. (2008). Prediction of work-hardening coefficient and exponential by adaptive inverse finite element method for tubular material. *J. Mater. Process. Tech.*, 20(1–3), 413–418.
- [8] Azizi (2009). Different implementations of inverse finite element method in sheet metal forming. *Mater. Design.*, 30(11), 2975–2980.
- [9] Gherlone, M., Cerracchio, P., Mattone, M. (2012). Shape sensing of 3D frame structures using an inverse Finite Element Method. *Int. J. Solids. Struct.*, 49(22), 3100–12.
- [10] Tessler, A., Spangler, J.L. (2005). A least-squares variational method for full-field reconstruction of elastic deformations in shear-deformable plates and shells. *Comput. Method. Appl. M.*, 194(2–5), 327–339.
- [11] Gherlone, M., Cerracchio, P., Mattone, M. (2014). An inverse finite element method for beam shape sensing: theoretical framework and experimental validation. *Smart. Mater. Struct.*, 23(23), 045027.
- [12] Cerracchio, P., Gherlone, M., Tessler, A. (2015). Real-time displacement monitoring of a composite stiffened panel subjected to mechanical and thermal loads. *Meccanica*, 50(13), 2487–2496.
- [13] Kefal, A., Oterkus, E. (2016). Displacement and stress monitoring of a chemical tanker based on inverse finite element method. *Ocean. Eng.*, 112, 33–46.
- [14] Kefal, A., Oterkus, E. (2016). Displacement and stress monitoring of a Panamax containership using inverse finite element method. *Ocean. Eng.*, 119, 16–29.
- [15] Kefal, A., Mayang, J.B., Oterkus, E. (2018). Three dimensional shape and stress monitoring of bulk carriers based on iFEM methodology. *Ocean. Eng.*, 147, 256–267.
- [16] Kefal, A., Oterkus, E., Tessler, A. (2016). A quadrilateral inverse-shell element with drilling degrees of freedom for shape sensing and structural health monitoring. *Eng. Sci. Technol. Int. J.*, 19(3), 1299–1313.
- [17] Kefal, A., Tessler, A., Oterkus, E. (2017). An enhanced inverse finite element method for displacement and stress monitoring of multilayered composite and sandwich structures. *Compos. Struct.*, 179, 514–540.
- [18] Kefal, A., Yildiz, M. (2017). Modeling of Sensor Placement Strategy for Shape Sensing and Structural Health Monitoring of a Wing-Shaped Sandwich Panel Using Inverse Finite Element Method. *Sensors*, 17(15), 2775.
- [19] Gherlone, M., Cerracchio, P., Mattone, M. (2018). Shape sensing methods: Review and experimental comparison on a wing-shaped plate. *Prog. Aerosp. Sci.*, <https://doi.org/10.1016/j.paerosci.2018.04.001>.
- [20] Fang, L., Chen, T., Li, R. (2016). Application of Embedded Fiber Bragg Grating (FBG) Sensors in Monitoring Health to 3D Printing Structures. *IEEE Sens. J.*, 16(20), 6604–10.
- [21] Papantoniou, A., Rigas, G., Alexopoulos, N.D. (2011). Assessment of the strain monitoring reliability of fiber Bragg grating sensor (FBGs) in advanced composite structures. *Compos. Struct.*, 93(12), 2163–72.

- [22] Liu, Q., Yan, J., Pham, D.T. (2016). Identification and optimal selection of temperature-sensitive measuring points of thermal error compensation on a heavy-duty machine tool. *Int. J. Adv. Manuf. Technol.*, 85(1–4), 345–53.
- [23] Zhang, Y., Yang, W. (2016). Simultaneous precision measurement of high temperature and large strain based on twisted FBG considering nonlinearity and uncertainty. *Sensor. Actuat. A-Phys.*, 239, 185–95.
- [24] Jiang, H., Fan, K.G., Yang, J.G. (2014). An improved method for thermally induced positioning errors measurement, modeling, and compensation. *Int. J. Adv. Manuf. Technol.*, 75, 1279–1289.
- [25] Miao, E.M., Gong, Y.Y., Dang, L.C., Miao, J.C. (2014). Temperature sensitive point selection of thermal error model of CNC machining center. *Int. J. Adv. Manuf. Technol.*, 74, 681–691.
- [26] Liang, R.J., Ye, W.H., Zhang, H.H., Yang, Q.F. (2012). The thermal error optimization models for CNC machine tools. *Int. J. Adv. Manuf. Technol.*, 63, 1167–1176.
- [27] Kankarani Farahani, M., Bostan, Shirin, M., Assempour, A. (2014). Development of an inverse finite element method with an initial guess of linear unfolding. *Finite. Elem. Anal. Des.*, 79, 1–8.
- [28] Bostan Shirin, M., Assempour, A. (2014). Some improvements on the unfolding inverse finite element method for simulation of deep drawing process. *Int. J. Adv. Manuf. Technol.*, 72(1–4), 447–56.
- [29] Cerracchio, P., Gherlone, M., Di Sciuva, M. (2015). A novel approach for displacement and stress monitoring of sandwich structures based on the inverse Finite Element Method. *Compos. Struct.*, 127, 69–76.
- [30] Du, F., Wang, X., Yao, M. (2014). Analysis of the non-uniform thermal behavior in slab continuous casting mold based on the inverse finite-element model. *J. Mater. Process. Tech.*, 214(14), 2676–2683.